NASA/TM-20205001422

Corrosion Behavior of Stainless Steel 304 and Nickel 625 Under Iodine Vapor at 300 °C

Gustavo Costa
HX5, LLC, Fort Walton Beach, Florida

Gabriel F. Benavides and Michael J. Kulis
Glenn Research Center, Cleveland, Ohio

John Setlock
The University of Toledo, Toledo, Ohio

June 2020

NASA STI Program . . . in Profile

Since its founding, NASA has been dedicated to the advancement of aeronautics and space science. The NASA Scientific and Technical Information (STI) Program plays a key part in helping NASA maintain this important role.

The NASA STI Program operates under the auspices of the Agency Chief Information Officer. It collects, organizes, provides for archiving, and disseminates NASA's STI. The NASA STI Program provides access to the NASA Technical Report Server—Registered (NTRS Reg) and NASA Technical Report Server—Public (NTRS) thus providing one of the largest collections of aeronautical and space science STI in the world. Results are published in both non-NASA channels and by NASA in the NASA STI Report Series, which includes the following report types:

- TECHNICAL PUBLICATION. Reports of completed research or a major significant phase of research that present the results of NASA programs and include extensive data or theoretical analysis. Includes compilations of significant scientific and technical data and information deemed to be of continuing reference value. NASA counter-part of peer-reviewed formal professional papers, but has less stringent limitations on manuscript length and extent of graphic presentations.

- TECHNICAL MEMORANDUM. Scientific and technical findings that are preliminary or of specialized interest, e.g., "quick-release" reports, working papers, and bibliographies that contain minimal annotation. Does not contain extensive analysis.

- CONTRACTOR REPORT. Scientific and technical findings by NASA-sponsored contractors and grantees.

- CONFERENCE PUBLICATION. Collected papers from scientific and technical conferences, symposia, seminars, or other meetings sponsored or co-sponsored by NASA.

- SPECIAL PUBLICATION. Scientific, technical, or historical information from NASA programs, projects, and missions, often concerned with subjects having substantial public interest.

- TECHNICAL TRANSLATION. English-language translations of foreign scientific and technical material pertinent to NASA's mission.

For more information about the NASA STI program, see the following:

- Access the NASA STI program home page at http://www.sti.nasa.gov

- E-mail your question to help@sti.nasa.gov

- Fax your question to the NASA STI Information Desk at 757-864-6500

- Telephone the NASA STI Information Desk at 757-864-9658

- Write to:
  NASA STI Program
  Mail Stop 148
  NASA Langley Research Center
  Hampton, VA 23681-2199

NASA/TM-20205001422

Corrosion Behavior of Stainless Steel 304 and Nickel 625 Under Iodine Vapor at 300 °C

Gustavo Costa
HX5, LLC, Fort Walton Beach, Florida

Gabriel F. Benavides and Michael J. Kulis
Glenn Research Center, Cleveland, Ohio

John Setlock
The University of Toledo, Toledo, Ohio

National Aeronautics and
Space Administration

Glenn Research Center
Cleveland, Ohio 44135

June 2020

This report is a formal draft or working paper, intended to solicit comments and ideas from a technical peer group.

This report contains preliminary findings, subject to revision as analysis proceeds.

Level of Review: This material has been technically reviewed by technical management.

Available from

NASA STI Program
Mail Stop 148
NASA Langley Research Center
Hampton, VA 23681-2199

National Technical Information Service
5285 Port Royal Road
Springfield, VA 22161
703-605-6000

This report is available in electronic form at http://www.sti.nasa.gov/ and http://ntrs.nasa.gov/

Corrosion Behavior of Stainless Steel 304 and Nickel 625 Under Iodine Vapor at 300 °C

Gustavo Costa*
HX5, LLC
Fort Walton Beach, Florida 32548

Gabriel F. Benavides and Michael J. Kulis
National Aeronautics and Space Administration
Glenn Research Center
Cleveland, Ohio 44135

John Setlock
The University of Toledo
Toledo, Ohio 43606

Summary

The chemical, structural, and microstructural behavior of stainless steel 304 (SS 304) and nickel 625 (Ni 625) were probed after exposure to iodine vapor laminar flow at 300 °C. This work was conducted in support of the development of in-space propulsion utilizing iodine as a propellant. The kinetics of corrosion was measured in a custom-built iodine-compatible thermogravimetric analyzer rig at 300 °C in which samples were exposed to an iodine laminar vapor flow of 1 $mg \cdot min^{-1}$ (carried by 20 $mL \cdot min^{-1}$ argon gas) for up to 31 days. Samples were characterized after the experiment by X-ray diffraction, electron microscopy, energy dispersive X-ray spectroscopy, and dynamic secondary ion mass spectrometry. All samples formed scales consisting mainly of metal oxyiodides showing different chemistry, microstructure, and crystalline phases. The paralinear rate law best describes the kinetics of oxidation of the samples. SS 304 exhibited slightly slower kinetics of oxidation ($106 \pm 3 \cdot 10^{-5}$ $mg \cdot cm^{-2} \cdot day^{-1}$) than Ni 625 ($122 \pm 3 \cdot 10^{-5}$ $mg \cdot cm^{-2} \cdot day^{-1}$) in the low-oxygen and low-water environment.

Introduction

NASA and the U.S. Air Force, amongst others, have been exploring the use of iodine as a propellant for Hall-effect and gridded-ion thrusters (Refs. 1 to 4). For example, NASA funded two recent projects to advance iodine technology sufficiently to demonstrate system-level solutions (thruster, cathode, feed system, and power processing unit). The iodine Satellite (iSat) project with a 200-W Hall-effect thruster (HET) was funded through NASA's Small Spacecraft Technology Program (SSTP) (Ref. 5), and a 600-W iodine Hall-effect propulsion system was demonstrated through the Advanced In-Space Propulsion (AISP) project funded through NASA's Game Changing Development Program (Ref. 6). NASA has also made various investments in iodine technologies and subsystems through the Small Business Innovation Research (SBIR) program (Ref. 7).

The primary advantage of iodine-based propulsion is the high propellant mass storage capability for a volume-constrained spacecraft that requires a large total impulse (Ref. 8). The storage density of iodine is 4.94 $g \cdot mL^{-1}$ (not accounting for ullage and voids), compared with no better than about 1.6 $g \cdot mL^{-1}$ for xenon. When a spacecraft is limited by volume constraints, such as imposed by a CubeSat deployer, the most straightforward means to increase propellant mass fraction is by utilizing a propellant with a high

*Employed by the NASA Glenn Research Center at the time of publication.

storage density. Another advantage of iodine, compared with propellants such as xenon and krypton, is a very low storage pressure. The low vapor pressure of iodine at room temperature (< 1 torr) has the potential to reduce tank and feed system launch safety concerns. In contrast, high-pressure propellants may be stored in excess of $1 \cdot 10^5$ torr, which can result in complex and costly verification testing. Furthermore, the low cost of iodine, due to its abundance on Earth compared to that of xenon, is attractive. Given the typical small scale of volume-constrained spacecraft, the propellant cost is not necessarily a significant concern compared with other spacecraft development costs. However, some futuristic concepts may envision use of iodine for very large spacecraft, where the propellant cost would become important. Unfortunately, even though the benefits described make iodine an intriguing propellant for volume-constrained missions, material compatibility of iodine is a major concern that must first be addressed: Iodine is known to be reactive with most spacecraft materials.

Understanding the compatibility of materials used in iodine propulsion systems, spacecraft, and ground test facilities is critical for both safe development and in-flight operations. Although a large body of research does exist on iodine-material compatibility in general, previous testing typically assumed the relevant environment as terrestrial. Minimal literature exists addressing environments relevant to in-space propulsion, where oxygen and water are typically not present. The reactivity between iodine vapor and some materials relevant to spacecraft and ground facilities has been previously investigated in a low-oxygen environment by Costa, Benavides, and Smith (Ref. 9). Several metallic materials including steels (304, 316, and A36), a titanium-aluminum alloy (Ti-Al, 6Al-4V), an aluminum-magnesium alloy (Al-Mg, 6061), and silicon-based coatings (Silcolloy® and Dursan® (SilcoTek Corporation)) were characterized after exposure to an iodine laminar vapor flow of 1 $mg \cdot min^{-1}$ (carried by 145 $mL \cdot min^{-1}$ argon gas) for 5, 15, and 30 days in a custom-built iodine vapor rig (IVR) at 300 °C. The austenitic steels showed a much thinner scale consisting of (Fe, Cr, and Ni) oxides when compared to carbon steel A36. The aluminum-magnesium alloy showed a thin scale consisting of mainly aluminum, iodine, and oxygen. The titanium-aluminum alloy showed no detectable scale. Some of these materials showed no oxidation after application of a silicon-based coating. It should be noted that although the iodine was carried by high-purity argon in these earlier investigations, the test setup likely involved the presence of oxygen and water at levels higher than anticipated, which may have led to much higher rates of corrosion than would be observed in the vacuum of space.

The goal of the work described here is to continue compatibility studies of iodine with common spacecraft and test facility materials, and improve the analytical capabilities by building an iodine-compatible thermogravimetric analyzer rig (TGA rig) for measuring the kinetics of corrosion of relevant materials by iodine. The new test facility also improved on previous test setups to reduce oxygen and water vapor infiltration. For the study described in this report, stainless steel 304 (SS 304, a common test facility alloy) and nickel 625 (Ni 625, a potential propulsion system alloy with good corrosion resistance) were selected for further investigation. The weight changes of these alloys were continuously measured under iodine laminar flow at 300 °C for up to 31 days in a low-oxygen and low-humidity environment. Samples were characterized after the experiment by X-ray diffraction (XRD), electron microscopy, energy dispersive X-ray spectroscopy (EDS), and secondary ion mass spectroscopy (SIMS).

Experimental Setup

Materials

SS 304 and Ni 625 sheets were purchased from a commercial vendor and each cut into square shapes 1.28 by 1.28 by 0.15 cm with a single 0.18-cm hole, resulting in coupon samples with total surface area of 4.08 cm^2 and weighing ~2 g. The coupon samples were cleaned with a detergent solution, rinsed with deionized water, and further cleaned in ultrasonic acetone and ethanol baths prior to the experiments.

Thermogravimetric Analysis Under Iodine Laminar Flow

The corrosion of the samples was investigated by a custom-made TGA rig as illustrated in Figure 1. Here, high-purity argon carrier gas flows at 20 mL·min^{-1} through a storage tank containing solid/vapor iodine heated at ~50 °C. Iodine vapor is carried by argon through heated stainless steel lines kept at ~110 °C and the quartz tube inserted in a tubular furnace heated at 300 °C. Iodine vapor was retained as potassium triiodide in a 0.1 mol·L^{-1} potassium iodide solution. The iodine flow was continuously monitored with an optical spectrometer. All stainless steel tubing and fittings were silicon coated to minimize reactivity with iodine vapor. Samples were directly suspended from a Cahn 1000 microbalance using a platinum hangwire and inserted in a quartz tube of a vertical tubular furnace. The furnace was sealed and flushed with argon while the temperature was raised to 300 °C and maintained for about 1 h before introducing the iodine laminar flow. The samples were exposed to an iodine laminar vapor flow of 1 mg·min^{-1} at ~15 psi (carried by the argon gas) for up to 31 days. A portable multicomponent gas analyzer (Ref. 10) was connected to the outlet of the rig during an experiment running only argon to measure the oxygen and water content in the system. The oxygen and water contents determined in the system were 2.10±0.02 and 0.90±0.01 percent, respectively. The weights of the samples were normalized to the unit area by dividing the weight gain by the total area of a particular sample. This analysis was used to determine weight change per area of the samples due to chemical reactions occurring between the iodine vapor and the alloy.

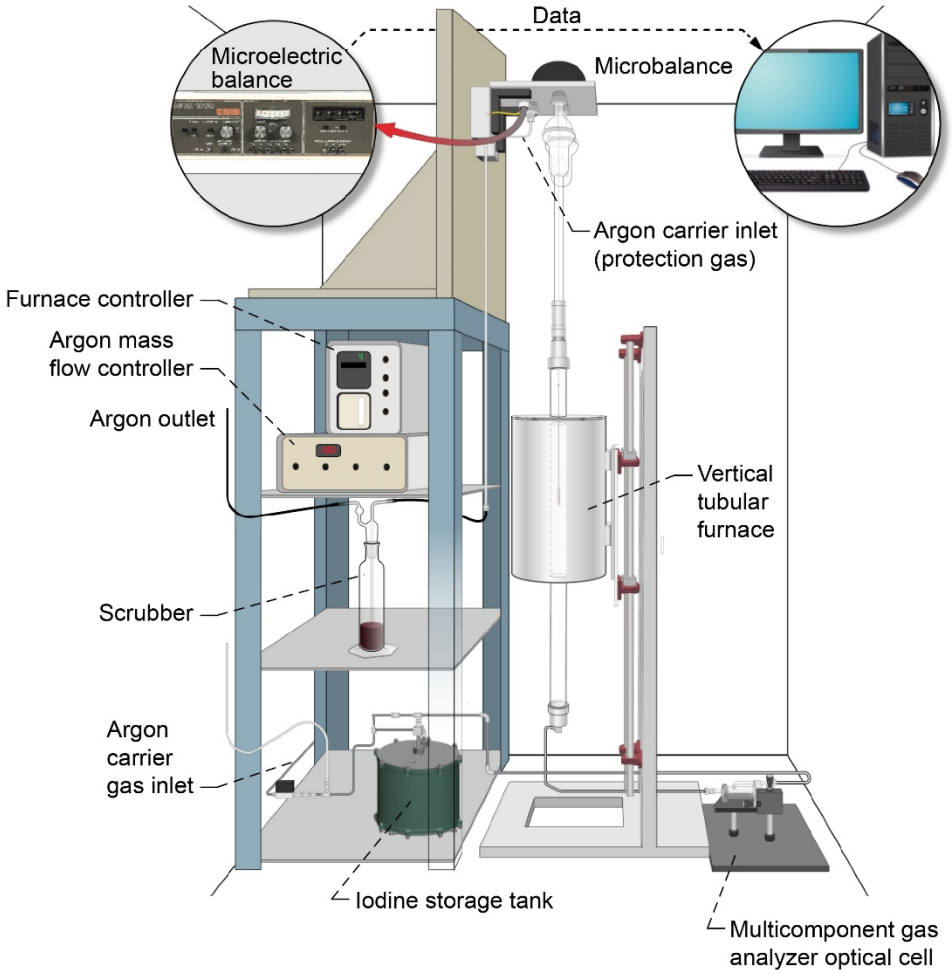

Figure 1.—Thermogravimetric analyzer rig (TGA rig) system.

Sample Characterization

The microgeometric characteristic roughness of the samples was measured by a Newview™ NX2 optical three-dimensional (3D) surface profilometer (Zygo Corporation). Chemical compositions of the as-received samples were measured by X-ray fluorescence analysis using a portable Niton™ XL3 X-ray fluorescence (XRF) analyzer (Thermo Fisher Scientific). XRD data of the samples after iodine exposure were acquired on a D8 DISCOVER diffractometer (Bruker-AXS GmbH) from 10° to 120° 2θ with a step size of 0.020° and a collection time of 2.5 $s \cdot step^{-1}$. The samples were mounted on zero background holders that rotated at 30 rpm. The diffractometer operated at an accelerating voltage of 40 kV and emission current of 40 mA with Cu-Kα radiation (λ = 0.154059 nm). Crystalline phases were identified using JADE 2010 v.3 software (Materials Data, Inc.) equipped with the International Centre for Diffraction Data (ICDD) Powder Diffraction File (PDF-4+, 2019). Elemental depth profile of the samples were measured by SIMS using a Cameca 6f spectrometer at Cerium Labs, Texas. Primary ions of cesium were used to sputter and analyze oxygen and iodine. Primary oxygen was used in the analysis of Fe, Cr, Ni, and Mo. Cross-sectional scanning electron microscopy (SEM) and elemental mapping analysis by EDS on the coupon samples after iodine exposure were performed in a TESCAN MAIA3 Triglav™ scanning electron microscope (TESCAN ORSAY HOLDING) equipped with an X-Max^N energy-dispersive X-ray silicon drift detector (EDS-SDD) (Oxford Instruments). Samples were mounted in a PolyFast® (Struers, Inc.) resin and polished to a mirror finish in nonaqueous solution prior to SEM-EDS.

Results

Surface Roughness and Elemental Analysis Before Exposure

The chemical composition of the SS 304 and Ni 625 coupon samples analyzed by XRF is provided in Table I. For SS 304 the average roughness measured on each side of the coupon sample was 0.249 and 0.232 μm, and for Ni 625 it was 0.225 and 0.203 μm.

TABLE I.—CHEMICAL COMPOSITION OF STAINLESS STEEL 304 AND NICKEL 625 COUPON SAMPLES

Element	Weight, percent	
	SS 304	Ni 625
Fe	70.2±0.3	4.46±0.03
Cr	18.19±0.09	19.70±0.05
Ni	8.0±0.1	63.66±0.06
Mn	1.85±0.07	0.37±0.03
Si	0.5±0.05	----------
Cu	0.36±0.03	0.12±0.02
Co	0.33±0.09	0.08±0.02
Mo	0.281±0.006	8.09±0.02
V	0.09±0.02	0.07±0.01
W	0.06±0.02	----------
Ti	0.06±0.03	0.17±0.02
Sn	0.02±0.02	0.009±0.004
Nb	----------	3.2±0.01
Zn	----------	0.042±0.007

Thermogravimetric Analysis and Kinetics of Corrosion

Figure 2 and Figure 3 show the weight change per area of the SS 304 and Ni 625 samples, respectively, continuously measured by thermogravimetric analysis. For comparison purposes, the data of the same materials from previous studies (Refs. 9 and 11) obtained by weighting the samples after they were exposed to same iodine flow in a furnace iodine rig are also provided in the plots. In the present study, a weight gain per area was initially observed for the SS 304 and Ni 625 samples exposed to iodine laminar flow followed by continuous weight loss. The weight change per area following a parabolic behavior for SS 304 and Ni 625 samples increased up to 0.5 and 4 days, respectively. This weight gain is

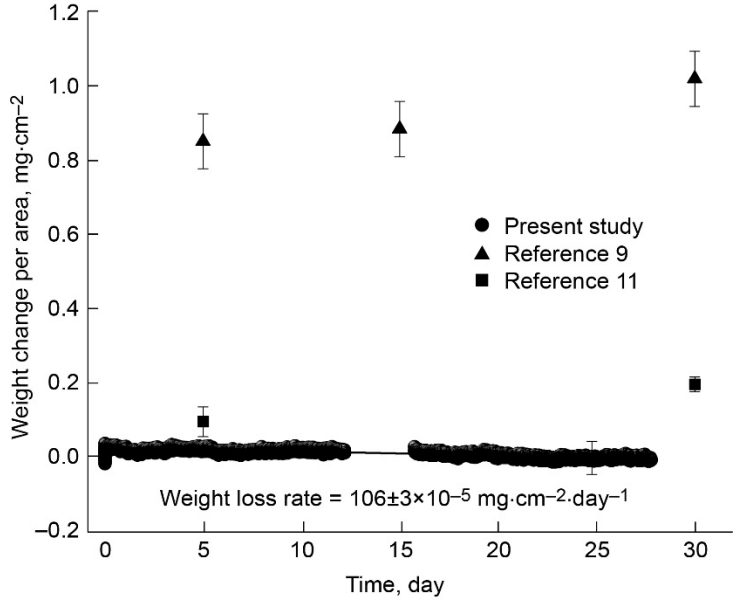

Figure 2.—Weight change per area versus time for stainless steel 304 (SS 304) samples exposed to iodine laminar flow at 300 °C.

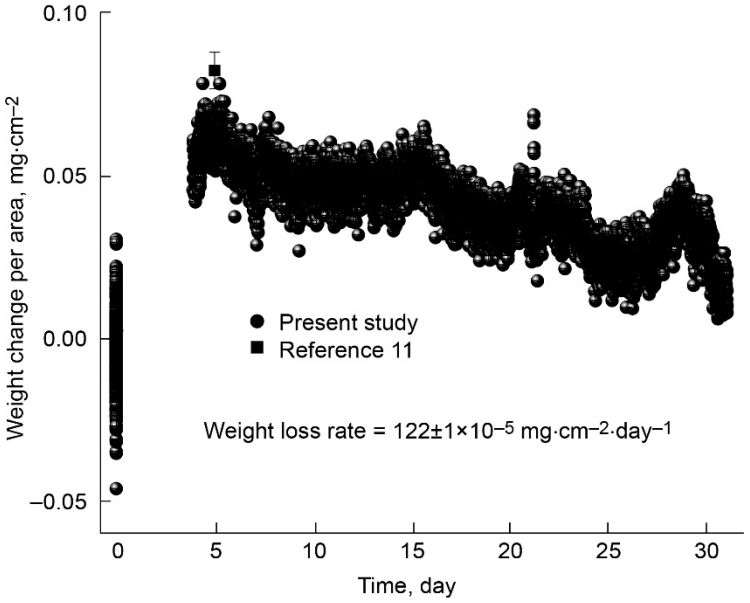

Figure 3.—Weight change per area versus time for nickel 625 (Ni 625) alloy exposed to iodine laminar flow at 300 °C.

usually related to scale or oxide growth resulting from oxidation of the alloys caused by the residual 2.1 percent oxygen and 0.9 percent H_2O present in the system. The weight loss of the samples after weight gain is usually related to volatilization of iodides. The weight loss rate calculated from the slope of the linear regression of the data points in the plots of Figure 2 and Figure 3 are $106\pm3\cdot10^{-5}$ mg·cm^{-2}·day^{-1} for the SS 304 sample and $122\pm3\cdot10^{-5}$ mg·cm^{-2}·day^{-1} for Ni 316. Linear regression fits were performed using OriginPro software version 9.5 (OriginLab Corporation, 2018), by propagating uncertainties from thermogravimetry and sample dimensions to weight data during fitting. In Figure 2, weight gain is observed for the SS 304 samples exposed to iodine in furnace tests (Refs. 9 and 11) considering the same exposure time instead of the weight loss observed in the current work. The data points of the Ni 625 sample measured in this work (Figure 3) are the same within the experimental uncertainties as the two data points measured in the previous study by Ramji, Benavides, and Costa (Ref. 11) carried out in an iodine furnace rig.

Surface and Cross Section Microstructural Characterization and Phase Analysis

The elemental depth profile obtained by EDS on the cross section of the SS 304 and Ni 625 samples exposed to iodine laminar flow at 300 °C for 28 and 31 days, respectively, are shown in Figure 4 and Figure 5. Elemental depth profiling was carried out along the yellow line shown on the electron images

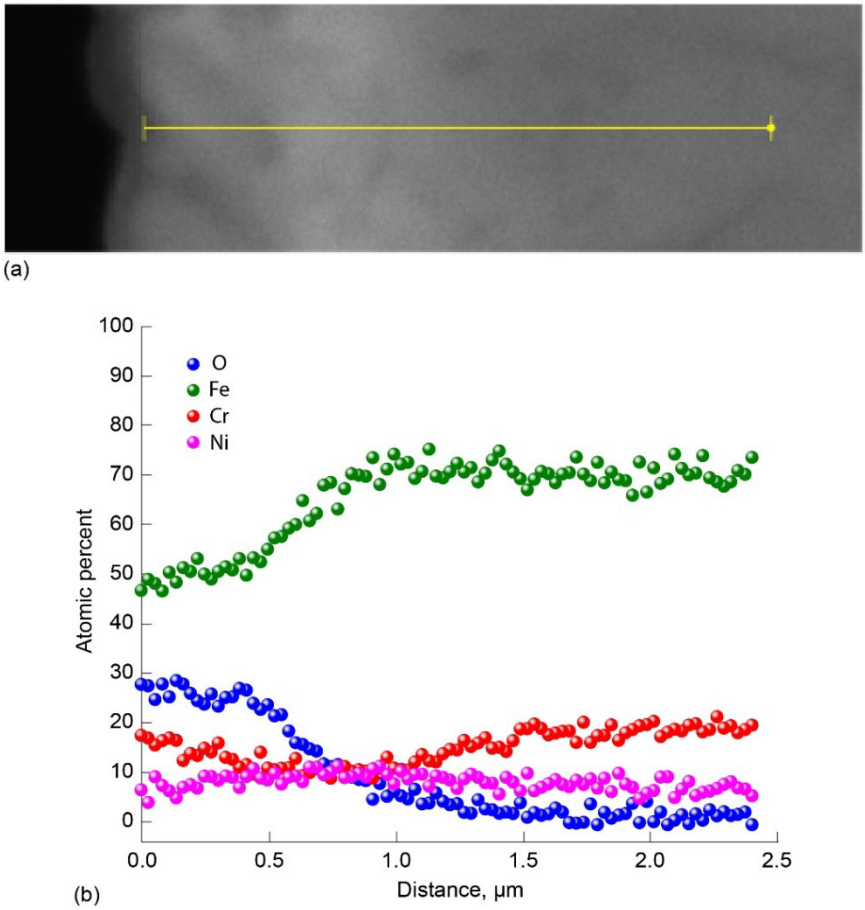

Figure 4.—Energy dispersive X-ray spectroscopy analysis of SS 304 sample exposed to iodine laminar flow at 300 °C in TGA rig for 28 days. (a) Yellow scan line of sample. (b) Elemental depth profile.

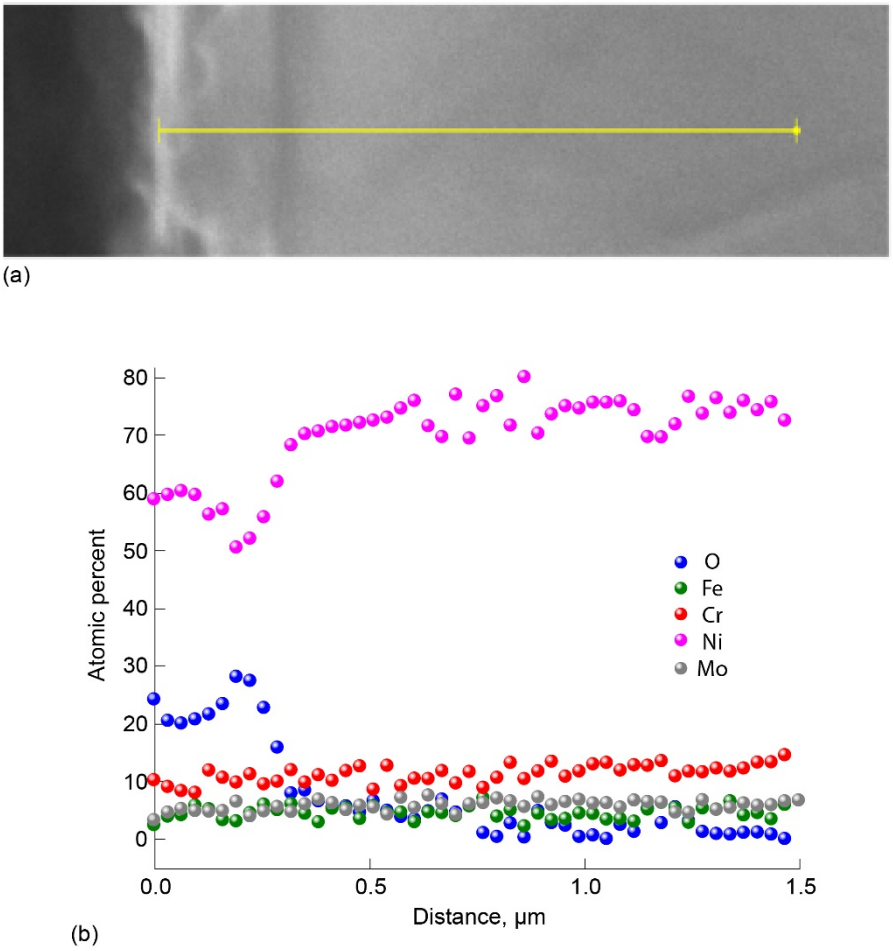

Figure 5.—Energy dispersive X-ray spectroscopy analysis of Ni 625 sample exposed to iodine laminar flow at 300 °C in TGA rig for 31 days. (a) Yellow scan line of sample. (b) Elemental depth profile.

above the depth profile graphs. Figure 4 indicates the SS 304 sample scale consists of one ~0.5-μm layer mainly composed of iron (47 to 53 at.%) and oxygen (23 to 29 at.%) with lower amounts of chromium (9 to 18 at.%) and nickel (4 to 11 at.%). Figure 5 indicates the Ni 625 sample consists of one ~0.2-μm layer mainly composed of nickel (50 to 60 at.%) and oxygen (20 to 28 at.%) with lower amounts of chromium (8 to 12 at.%), iron (3 to 6 at.%), and molybdenum (4 to 6 at.%).

The elemental depth profile of the unexposed and exposed SS 304 and Ni 625 samples characterized by SIMS are shown in Figure 6 and Figure 7, respectively. The unexposed (as-received) SS 304 sample (Figure 6(a)) is oxidized at the surface (~100 nm), as evident from the high concentration of oxygen (10^{20} atoms·cm^{-3} range near the surface). The surface of the exposed SS 304 sample to approximately 0.3 μm in depth exhibits higher concentrations of oxygen and iodine and higher intensities of chromium and iron and a lower intensity of nickel. After 0.3 μm depth, the concentration and intensity of these elements decrease to background levels. The SIMS analysis indicates that the surface layer of the exposed SS 304 sample consists of iron chromium nickel iodine oxide. Iodine is present in the oxide scale at trace levels, since its concentration is 3 orders of magnitude lower than oxygen. Near the surface (~0.3 μm), this scale becomes depleted of nickel. The analysis on the unexposed Ni 625 sample detected chromium at the surface of alloy. From the surface to ~0.15 μm depth, the unexposed Ni 625 sample exhibits a high

intensity of chromium. Near the surface to 0.2 μm depth, the exposed Ni 625 sample exhibits high concentrations of oxygen and iodine as well as high intensities of nickel, chromium, iron, and molybdenum. The concentrations of iodine and oxygen gradually decrease with depth from the surface to ~3 and ~7 μm, respectively, and the intensities of Ni, Fe, Cr, and Mo sharply decrease from the surface to ~0.3 μm. The SIMS analysis reveals that the scale formed on the Ni 625 exposed sample consists of nickel oxide with lower amounts of iodine, chromium, iron, and molybdenum.

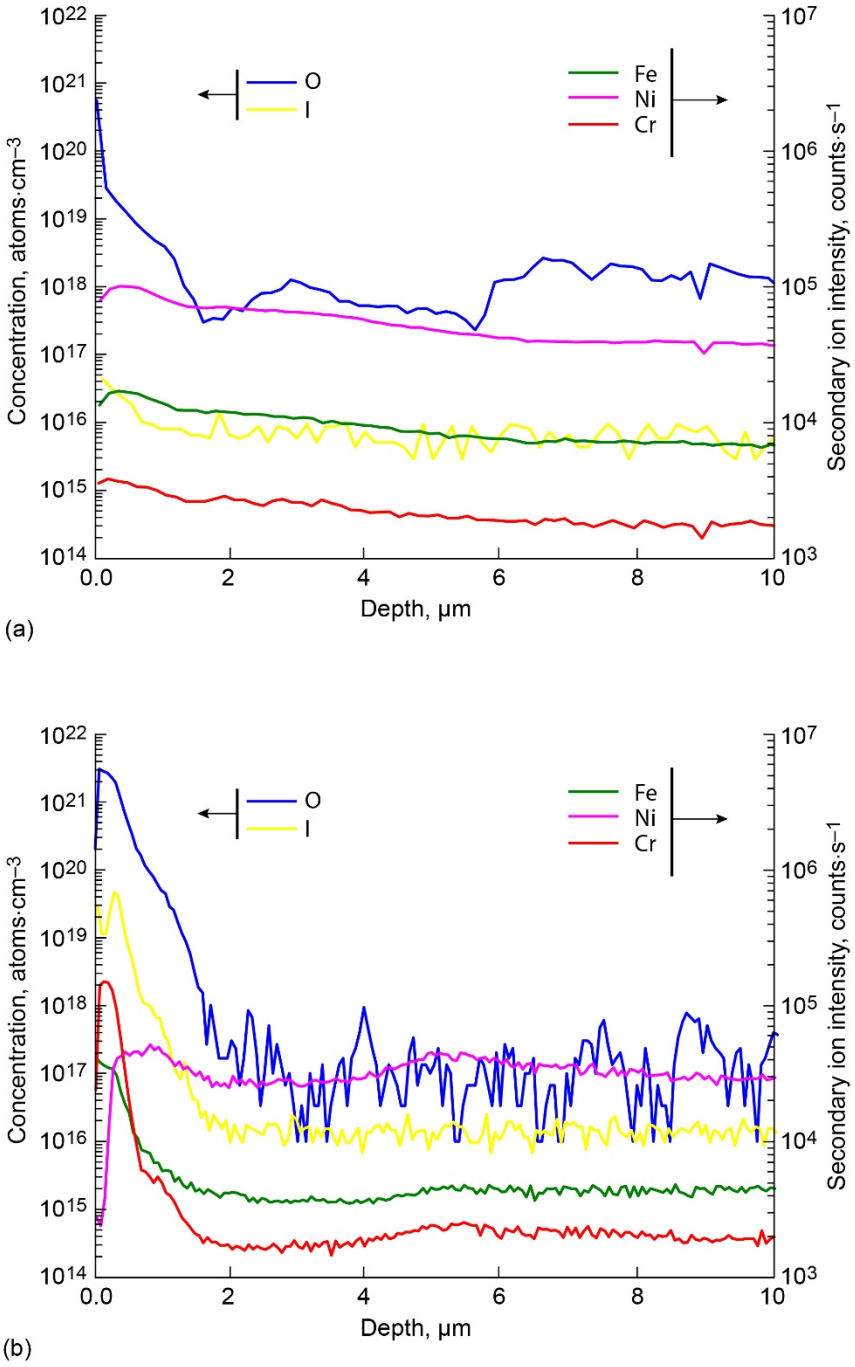

Figure 6.—Secondary ion mass spectroscopy measured depth profiles of O and I with qualitative depth profiles of Fe, Ni, and Cr for SS 304 samples. (a) Unexposed. (b) Exposed to iodine laminar flow at 300 °C in TGA rig for 28 days.

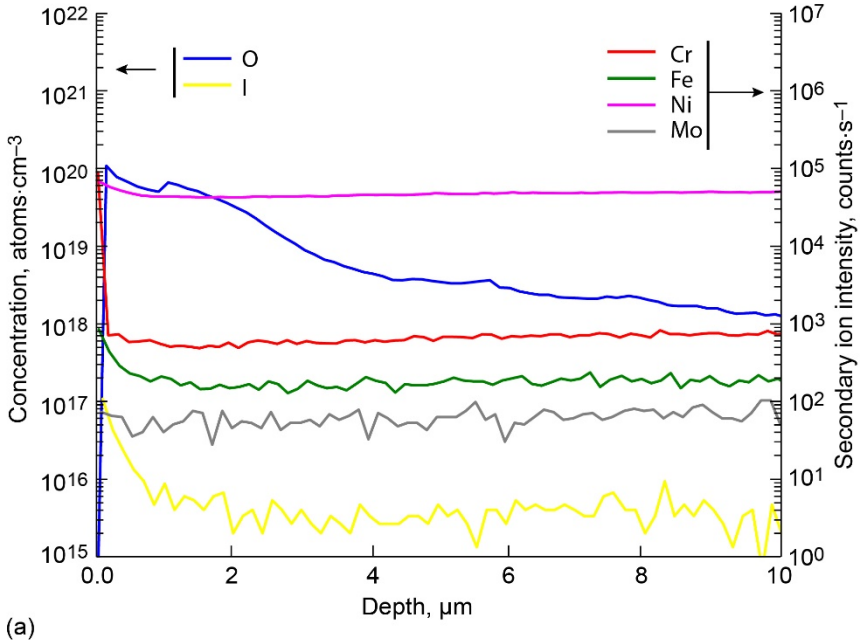

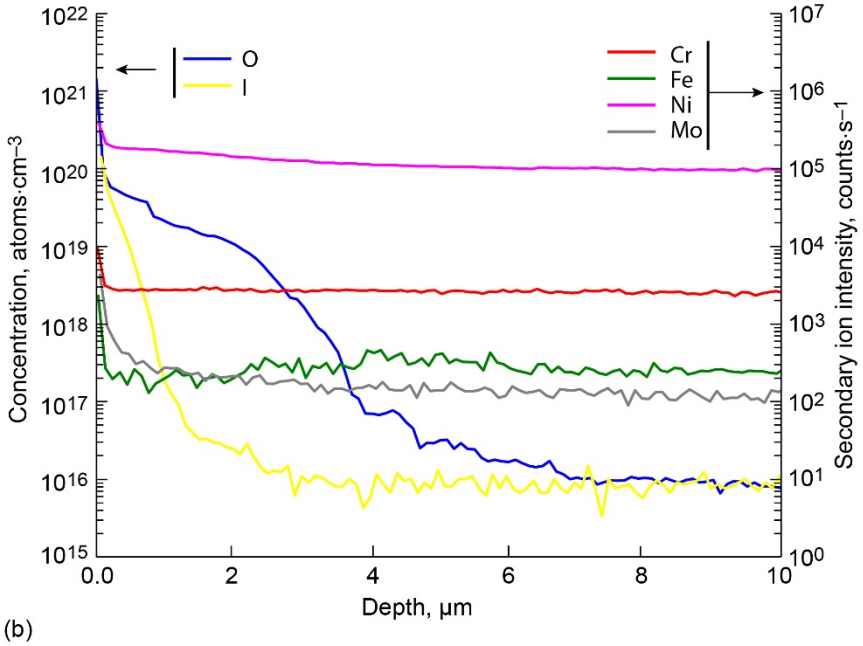

Figure 7.—Secondary ion mass spectroscopy measured depth profiles of O and I with qualitative depth profiles of Fe, Ni, and Cr of Ni 625 samples. (a) Unexposed. (b) Exposed to iodine laminar flow at 300 °C in TGA rig for 31 days.

The XRD patterns of the SS 304 and Ni 625 samples exposed to iodine are presented in Figure 8 and Figure 9. The phases detected in the samples with their space groups and PDF cards are listed in Table II. Four phases were detected in the SS 304 sample: ferrite (cubic α-Fe), chromium iron oxide (rhombohedral $Fe_{0.2}Cr_{1.8}O_3$), spinel (cubic $FeCr_2O_4$), and nickel chromium oxide (cubic $Ni_{0.7}Cr_{0.3}O_{0.65}$), in addition to the main austenite (γ-Fe) phase. Only the austenite (γ-Ni) was detected on the exposed Ni 625 sample.

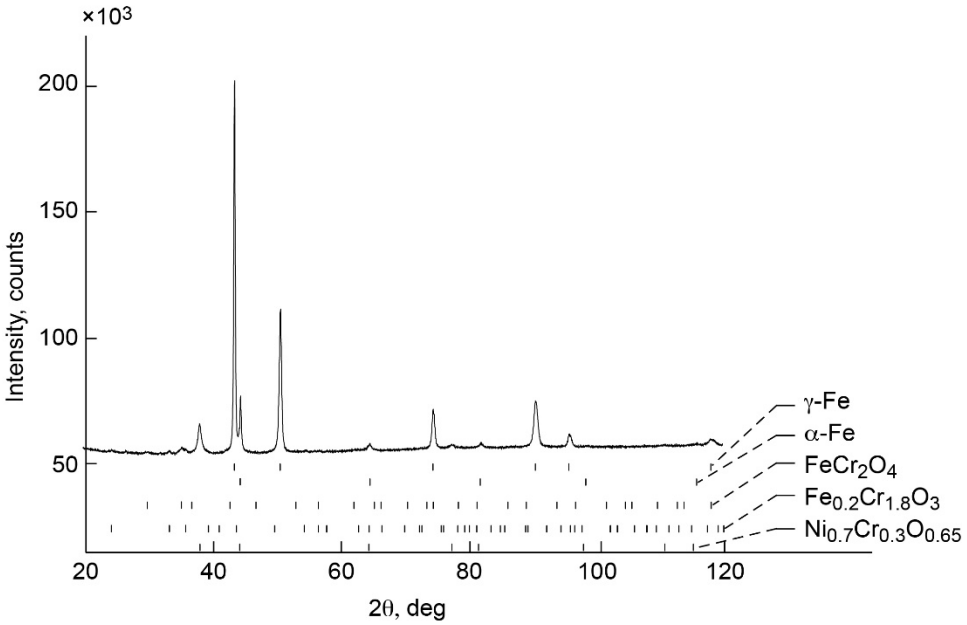

Figure 8.—X-ray diffraction patterns of SS 304 sample exposed to iodine vapor laminar flow for 28 days.

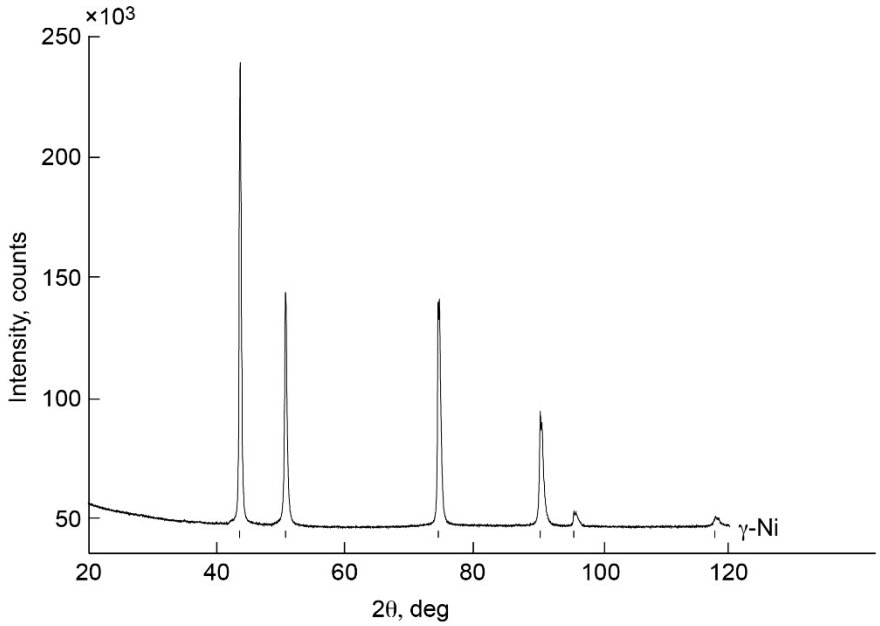

Figure 9.—X-ray diffraction patterns of Ni 625 sample exposed to iodine vapor laminar flow for 31 days.

TABLE II—PHASES DETECTED IN SS 304 AND Ni 625 SAMPLES WITH THEIR SPACE GROUPS AND PDF CARDS

Phase	Space group, PDF card	
	SS304	Ni 625
Austenite, γ-Fe	Fm3m, 04-014-0264	----------
Ferrite, α-Fe	Im3m, 03-065-7753	----------
Spinel, $FeCr_2O_4$	Fd3m, 04-016-4072	----------
$Fe_{0.2}Cr_{1.8}O_3$	R3c, 04-006-8202	----------
$Ni_{0.7}Cr_{0.3}O_{0.65}$	Fm3m, 04-011-9040	----------
Ni, γ-Ni	----------	Fm3m, 98-001-6416

Discussion

The results obtained from SEM-EDS, SIMS, and XRD for SS 304 and Ni 625 indicate that their corrosion product, or scale, is mainly composed of metal oxyiodides in which iodine is present at trace levels. The presence of iodine in the oxide phases detected by XRD is evident from SIMS as shown in the elemental depth profiles of Figure 6 and Figure 7. For SS 304, iodine may be present in the solid solution of one or all oxide phases ($FeCr_2O_4$, $Fe_{0.2}Cr_{1.8}O_3$, and $Ni_{0.7}Cr_{0.3}O_{0.65}$) detected by XRD analysis. For Ni 625, iodine is present in the nickel oxide although its phase was not detected by XRD. The 2.1 percent water and 0.9 percent oxygen present in our system was enough to cause the oxidation of the alloy. Our findings on SS 304 sample corroborated with those reported by Wren, Glowa, and Merritt (Ref. 12). They proposed that corrosion of stainless steel exposed to a continuous flow of nitrogen or air containing iodine at room temperature is catalyzed by iodine. The measured relative humidity in their system was about 32 to 35 percent. The surfaces of the exposed samples in the work reported by Wren, Glowa, and Merritt were characterized by EDS and by X-ray photoelectron spectroscopy (XPS). They found a preferential diffusion of iron and the formation of Fe-I-O, and proposed the following reactions between stainless steel, air, and iodine:

$$\mathrm{Fe_2 + I_2 = FeI_2} \tag{1}$$

$$\mathrm{FeI_2} + \frac{y}{2} = \mathrm{FeI}_x\mathrm{O}_y + \left(1 + \frac{x}{2}\right)\mathrm{I_2} \tag{2}$$

where FeI_xO_y is composed of iron iodides and iron oxides. They also stated that this FeI_xO_y phase mixture could react with more oxygen to release iodine or iodine is bound either in stable compounds or in film areas inaccessible to oxygen. Here, nickel from Ni 625 is assumed to preferentially react with iodine and oxygen to form nickel oxyiodide. Considering the findings of Wren et al. and of the current work, the reactions for SS 304 and Ni 625 are postulated to be the following:

$$\mathrm{M_{alloy} + I_2(g) = MI_2(s)} \tag{3}$$

$$\mathrm{MI_2} + \frac{y}{2}\mathrm{O_2} = \mathrm{MI}_x\mathrm{O}_y + \left(1 - \frac{x}{2}\right)\mathrm{I_2} \tag{4}$$

where M is metal (M = Fe, Cr, Ni, and Mo).

The data points of the weight gain per area in Figure 2 and Figure 3 related to the corrosion of the samples would fit into a paralinear rate equation. The paralinear rate model previously described by Tredmon (Ref. 13) and Maloney and McNallan (Ref. 14) describes two simultaneous reactions leading to an increase and decrease in the sample mass through scale or oxide formation (parabolic) and its consumption (linear), respectively. The corrosion process of the samples of this work is initially governed by the formation of metal oxyiodides (Eq. (4)) and then by consumption of the metal from the alloy to form metal iodide (Eq. (2)). The vapor pressure of the iodides at 300 °C would be high enough to allow their vapor species to be carried by the iodine and argon laminar flow.

The fact that the SS 304 samples exposed to iodine in furnace tests Figure 2 exhibited weight gain instead of weight loss observed in this study for the same exposure time is related to the higher oxygen and water content in their system leading to more oxyiodides formation (scale formation). The corrosion of the SS 304 exposed to iodine in furnace rigs would be governed by Equation (2) and it would be best fitted into a parabolic rate law. The lower weight gain for the SS 304 sample described in the work by Ramji, Benavides, and Costa (Ref. 11) when compared to the work by Costa, Benavides, and Smith (Ref. 9) can be also related to the differences in the water and oxygen content in their systems, although they were not measured. The Ramji et al. experiment was carried out in the same rig used by Costa et al. except that the container to store and vaporize iodine was improved. The Erlenmeyer flask used to contain and vaporize iodine used by Costa et al. was replaced by a custom-made stainless steel iodine tank. Such improvement was enough to better seal the system against oxygen, which resulted in lower weight gain for the SS 304 samples in the work of Ramji et al., as shown in Figure 2. Furthermore, there is no difference between the data points for Ni 625 obtained in the furnace rig and TGA rig shown in Figure 3, implying that the corrosion mechanism of this sample is not strongly affected by the oxygen content in the system.

Conclusion

A scale consisting of metal oxyiodides formed on the base of stainless steel 304 (SS 304) and nickel 625 (Ni 625) exposed to an iodine and argon laminar flow with 2.1 percent water and 0.9 percent oxygen in the rig system. The corrosion of the alloys is governed by the reaction between the metals and iodine to form metal iodide volatile compounds, which are carried away by the laminar flow of iodine and argon at 300 °C. The oxidation of the samples are catalyzed by iodine, and it is sensitive to oxygen concentration. The kinetics of oxidation of the samples follow a paralinear rate law. SS 304 exhibited slower kinetics of oxidation ($106 \pm 3 \cdot 10^{-5}$ mg·cm^{-2}·day) than Ni 625 ($122 \pm 3 \cdot 10^{-5}$ mg·cm^{-2}·day).

References

1. Smith, Timothy D., et al.: Overview of NASA Iodine Hall Thruster Propulsion System Development. Presented at Space Propulsion, NASA TN30748, Rome, Italy, 2016. http://ntrs.nasa.gov
2. Hillier, Adam C.: Revolutionizing Space Propulsion Through the Characterization of Iodine as Fuel for Hall-Effect Thrusters. Master of Science thesis, Air Force Institute of Technology, 2011. https://scholar.afit.edu/etd/1329/ Accessed May 22, 2020.
3. Tsay, Michael, et al.: Maturation of Iodine-Fueled BIT–3 RF Ion Thruster and RF Neutralizer. AIAA 2016–4544, 2016.
4. Szabo, James, et al.: Performance Evaluation of an Iodine-Vapor Hall Thruster. J. Propul. Power, vol. 28, no. 4, 2012.

5. Polzin, Kurt A., et al.: System Development for the Iodine Satellite (iSAT) Demonstration Mission. IEPC–2015–09/ISTS–2015–b–09, 2015.
6. Benavides, Gabriel F., et al.: Iodine Hall-Effect Electric Propulsion System Research, Development, and System Durability Demonstration. AIAA 2018–4422, 2018.
7. Thompson, Seth J., et al.: Development of an Iodine Compatible Hollow Cathode. AIAA 2019–3997, 2019.
8. Dankanich, John W., et al.: Mission and System Advantages of Iodine Hall Thrusters. AIAA 2014–3905, 2014.
9. Costa, Gustavo C.C.; Benavides, Gabriel F.; and Smith, Timothy D.: Chemical, Structural and Microstructural Changes in Silicon-Based Coating Materials Exposed to Iodine Vapor. NASA/TM—2017-219498, 2017. http://ntrs.nasa.gov
10. Pilgrim, Jeffrey S., et al.: Optical Multi-Gas Monitor Technology Demonstration on the International Space Station. ICES–2014–058, 2014.
11. Ramji, Karpagavalli; Benavides, Gabriel F.; and Costa, Gustavo C.C.: Chemical and Microstructural Investigation of the Influence of Iodine Vapor on the Oxidation of Nickel Alloys at 300 °C. NASA Internship Final Report, internal document, 2018.
12. Wren, J.C.; Glowa, G.A.; and Merritt, J.: Corrosion of Stainless Steel by Gaseous I_2. J. Nucl. Mater., vol. 265, 1999, pp. 161–177.
13. Tredmon, C.S.: The Effect of Oxide Volatilization on the Oxidation Kinetics of Cr and Fe-Cr Alloy. J. Electrochem. Soc., vol. 113, 1966, pp. 766–768.
14. Maloney, M.; and McNallan, M.J.: The Effect of Chlorine on the Kinetics of Oxidation of Colbalt in Environments Containing 0.5 Atmosphere of Oxygen Between 900 K and 1200 K. Metall. Trans. B, vol. 16, 1985, pp. 751–761.